Electronic Supplementary Material (ESI) for Journal of Materials Chemistry C.

Supporting Information

Applications of hot-exciton molecules based anthracene and imidazole in integrated organic blue-emitting and ultraviolet photodetective device

Qiao Luo,[a] Yannan Gao,[b] Huixia Xu, *[a] Song Zhao,[a] Wenjian Dong,[a] Yanqin Miao,[a] Yating Wang,[a] Hua Wang,[a] and Junsheng Yu, *[b]

[a] Key Laboratory of Interface Science and Engineering in Advanced Materials, Ministry of Education, Taiyuan University of Technology, Taiyuan, 030024, China,

E-mail: xuhuixia@tyut.edu.cn

[b] State Key Laboratory of Electronic Thin Films and Integrated Devices, School of Optoelectronic Science and Engineering, University of Electronic Science and Technology of China (UESTC), Chengdu, 610054, PR China

E-mail: jsyu@uestc.edu.cn

1.Materials and methods

All the reagents and solvents used for the syntheses and measurements were purchased from commercial suppliers and were used without further purification unless otherwise noted. ^{1}H NMR and ^{13}C NMR spectra were measured with a Switzerland Bruker DR × 600.

UV-vis absorption spectra were measured using Lambda Bio 40. Mass spectral data were obtained using a Finnigan 4021C gas chromatography (GC)-mass

spectrometry (MS) instrument. The Photoluminescence (PL) spectra were recorded using HORIBA FluoroMax-4 spectrophotometer.

Thermogravimetric analysis (TGA) curves were undertaken using a Netzsch TG 209F3 under a dry nitrogen atmosphere heating from room temperature up to 800 ℃ at a rate of 10 ℃/min. Differential scanning calorimetry (DSC) was performed on a DSC Q2000 at a heating rate of 10 ℃/min from 40 to 300 ℃, then cooling down to room temperature rapidly, and heating up to 300 ℃ at a heating rate of 10 ℃/min again; the melting temperature (T_m) was obtained from the first heating scan and the glass transition temperature (T_g) was determined from the second heating scan.

Cyclic voltammetry (CV) was carried out in a solution of tetrabutylammonium perchlorate (0.1 M) in acetonitrile at a scan rate of 100 mV/s at room temperature using a conventional three electrode cell, which consisted of the working electrode platinum plate, the counter electrode platinum wire, and the reference electrode calomel electrode.

Powder X-ray diffraction were recorded using Single-crystal X-ray data were collected using a Bruker APEX-II CCD diffractometer with a graphite-monochromated Mo K_α radiation (λ = 0.71073 Å, Bruker Corporation, Billerica, MA, USA).

DFT calculation

Theoretical calculations were performed using the Gaussian 09 package. Geometry optimization was performed by density functional theory (DFT) in B3LYP/6-31G(d) basis sets. The natural transition orbitals (NTOs) are calculated by TD-B3LYP/6-31G(d) method.

OLED fabrication and characterization

The OLEDs with area of 3 × 3 mm^2 were fabricated by vacuum deposition onto the indium tin oxide (ITO) glass substrates. The substrates were cleaned, in the following order, with deionized water, acetone, and ethanol. The electroluminescence (EL) spectra and CIE coordinates were measured by a PR-655 spectrophotometer. The current density-voltage-luminance (J-V-L) characteristics of the OLEDs were recorded using Keithley 2400 Source Meter and ST-900M Spot Brightness Meter.

OLED-UVPD fabrication and characterization

All the devices were deposited on pre-cleaned indium tin oxide (ITO) glass substrates, which were consecutively cleaned by detergent, deionized water, acetone and isopropyl alcohol for 15 minutes at each ultrasonic step. Then they were treated in UV/ozone for 15 minutes to diminish the work function. After that, under a pressure of 2×10^{-4} Pa, the organic functional layer was vacuum deposited at a rate of 0.5-1 Å/s. At a vacuum degree of 3×10^{-3} Pa, the Mg:Ag metal cathode was deposited at a rate of about 10 Å/s without breaking the vacuum to form a device area of 0.1 cm^2. During the deposition process, the thickness and deposition rate of the material are monitored by an oscillating quartz crystal monitor.

Photoluminescence quantum yield (PLQY)

Photoluminescence quantum yield (PLQY) for thin film was measured using an integrating sphere apparatus. PLQY of different solutions were determined by using 0.1 M quinine sulfate as a reference (PLQY= 54.6%) and were calculated by using the following formula:

$$Q_x = Q_r\left(\frac{A_r(\lambda_r)}{A_x(\lambda_x)}\right)\left(\frac{I(\lambda_r)}{I(\lambda_x)}\right)\left(\frac{n_x^2}{n_r^2}\right)\left(\frac{D_x}{D_r}\right)$$

Where Q is the PLQY, A is the value of absorbance, I is the intensity of excitation source, n is the refractive index of solvent, D is the area of emission spectra, λ is the corresponding wavelength. The subscript r stands for the reference while x stands for test subject. The excitation wavelength is 398 nm. Radiative transition rate (k_r) and non-radiative transition rate (k_{nr}) were calculated according to the following formula:

$$k_r = \frac{\Phi}{\tau};$$

$$k_{nr} = \frac{1 - \Phi}{\tau}$$

(Φ: PLQY, τ: fluorescent lifetime).

Lippert-Mataga solvatochromic model

The influence of solvent polarity on the photophysical properties of DP and SP were analyzed by the Lippert-Mataga equation, which can describe the interactions between the solvent and the dipole moment of solute.

$$hc(\nu_a - \nu_f) = hc(\nu_a^0 - \nu_f^0) - \frac{2(\mu_e - \mu_g)^2}{a^3} f(\varepsilon, n)$$

where f is the orientational polarizability of the solvent; μe is the excited-state dipole moment; μg is the groundstate dipole moment; a is the solvent cavity (Onsager) radius, derived from the Avogadro number (N), molecular weight (M), and density (d = 1.0 g/cm^3); ε and n are the solvent dielectric and the solvent refractive index, respectively; and f (ε, n) and a can be calculated, respectively, as the following:

$$f(\varepsilon, n) = \frac{\varepsilon - 1}{2\varepsilon + 1} - \frac{n^2 - 1}{2n^2 + 1}$$

$$a = \left(\frac{3M}{4N\pi d}\right)^{\frac{1}{3}}$$

Space charge limited current (SCLC)

$$J = \frac{9\mu_0\varepsilon_0\varepsilon_r V^2}{8d^3}$$

where *d* is the thickness ofthe sample, ε_0 and ε_r are the vacuum dielectric permittivity and the dielectric constant of the material respectively, *V* is the electric field strength, *J* is the current density and μ_0 is the carrier mobility.

Detection rate (*D)**

detection rate (*D**) is widely used to characterize the sensitivity of photodetectors. If we assume that the shooting noise produced by dark current is the main contribution of noise, then the photodetector *D** can be calculated as in:

$$D^* = \frac{R}{(2qJ_{dark})^{\frac{1}{2}}} = \frac{(J_{light} - J_{dark})/P}{(2qJ_{dark})^{\frac{1}{2}}}$$

where *R* is the responsivity, and *P* is power efficiency of the ultraviolet source. J_{dark} and J_{light} are dark and photocurrent densities, respectively. The overall trend in UV detection performance is mainly due to the characteristics of J_{dark} and J_{light}.

2.Synthetic of compounds

CrAn-Br

4-Carbazol-9-ylbenzeneboronic acid (3.47 mmol, 0.52 g), 9,10-dibromoanthracene (2.61 mmol, 0.88 g), tetrakis (triphenylphosphine) palladium(0) ($Pd(PPh_3)_4$) (0.08 mmol, 100 mg), 2 M aqueous potassium carbonate (K_2CO_3) (10 mL) were dissolved in 20 mL of toluene and 20 mL of ethanol in a mixed solution. The reaction was slowly heated to 90 °C and the mixture was stirred under nitrogen for 3 h. The temperature of the reaction system was cooled to 25 °C. The ethanol and toluene were removed by spin evaporation and extracted by adding a mixture of water (50 mL) and CH_2Cl_2 (3×50 mL). The organic phase was dried by adding anhydrous magnesium sulphate and spun dry, and the crude product The crude product was purified by column chromatography using PE/DCM (4:1, V/V) as the eluent to give **CrAn-Br** as a pale-yellow solid in 65% yield. ^1H NMR (600 MHz, $CDCl_3$) δ 8.67 (d, J = 13.2 Hz, 2H), 8.22 (d, J = 11.4 Hz, 2H), 7.81 (t, J = 11.4 Hz, 4H), 7.69 – 7.63 (m, 6H), 7.52 (m, 4H), 7.36 (t, J = 10.8 Hz, 2H).

PPIAn1N

The synthesis of **PPIAn1N** was similar to that of CrAn-Br. The synthetic route is

shown in Scheme 1, with PE/DCM (1:1, V/V) as the eluent. The resulting product was recrystallized from DCM to give a white solid **PPIAn1N** in 55% yield. ^{1}H NMR (600 MHz, DMSO-d6) δ 9.02 – 8.88 (m, 2H), 8.78 (d, J = 7.8 Hz, 1H), 8.17 (dd, J = 37.2, 8.4 Hz, 2H), 8.04 – 7.65 (m, 10H), 7.56 (m, 7H), 7.47 – 7.10 (m, 8H), 6.92 (d, J = 8.4 Hz, 1H), 6.64 (m, 1H). ^{13}C NMR (100 MHz, $CDCl_3$) δ 149.73, 138.70, 137.83, 136.55, 135.58, 134.24, 132.66, 132.52, 130.38, 130.34, 129.56, 129.23, 128.94, 128.85, 128.71, 128.36, 128.32, 128.29, 128.21, 128.15, 127.29, 127.20, 127.11, 126.31, 126.24, 126.06, 125.82, 125.56, 125.30, 125.25, 124.98, 124.66, 124.56, 124.18, 123.93, 123.13, 122.13, 121.79, 119.90. MALDI-TOF (m/z): Calcd for $C_{51}H_{32}N_2$, 672.83; Found: 672.257 [M+].

PPIAn2N

The synthesis process of **PPIAn2N** was similar to that of CrAn-Br. The synthetic route is shown in Scheme 1, with PE/DCM (1:1, V/V) as the eluent and the resulting product recrystallized from DCM to give a white solid **PPIAn2N** in 60% yield. ^{1}H NMR (600 MHz, $CDCl_3$) δ 8.99 – 8.93 (d, J = 7.8 Hz, 1H), 8.81 (d, J = 8.4 Hz, 1H), 8.74 (d, J = 8.4 Hz, 1H), 8.07 (d, J = 8.4 Hz, 1H), 8.02 (dd, J = 7.2, 2.4 Hz), 7.98 – 7.95 (m, 1H), 7.93 – 7.90 (m, 1H), 7.85 (ddd, J = 8.4, 4.8, 2.4 Hz, 2H), 7.80 – 7.76 (t, J = 7.2 Hz, 1H), 7.73 – 7.66 (m, 10H), 7.62 – 7.56 (m, 3H), 7.54 (ddd, J = 13.8, 6.6, 1.2 Hz, 1H), 7.45 (ddd, J = 10.2, 7.2, 2.4 Hz, 2H), 7.36 – 7.28 (m, 5H), 7.28 – 7.25 (m, 1H). ^{13}C NMR (100 MHz,

$CDCl_3$)δ 149.72, 138.73, 137.83, 136.54, 136.13, 135.45, 135.38, 132.37, 131.74, 130.32, 129.24, 129.18, 128.97, 128.95, 128.83, 128.69, 128.48, 128.21, 127.31, 127.06, 126.95, 126.87, 126.32, 126.23, 126.04, 125.80, 125.42, 125.30, 125.22, 124.66, 124.11, 123.93, 123.13, 122.13, 122.07, 121.79, 119.89. MALDI-TOF (m/z): Calcd for $C_{51}H_{32}N_2$, 672.83; Found: 672.266 [M+].

PPIAnp

The synthesis of **PPIAnp** was similar to that of CrAn-Br. The synthetic route is shown in Scheme 1, with PE/DCM (1:1, V/V) as the eluent. The resulting product was recrystallized from DCM to give a pale yellow solid **PPIAnp** in 47% yield. ^{1}H NMR (600 MHz, $CDCl_3$) δ 8.99 – 8.94 (m, 1H), 8.81 (d, J = 8.4 Hz, 1H), 8.75 (d, J =7.8Hz, 1H), 7.88 – 7.82 (m, 2H), 7.79 (ddd, J = 13.8, 6.6, 0.6 Hz, 1H), 7.73 – 7.64 (m, 10H), 7.63 – 7.59 (m, 2H), 7.57 – 7.52 (m, 2H), 7.50 – 7.45 (m, 2H), 7.44 – 7.39 (m, 3H), 7.37 – 7.29 (m, 5H), 7.09 – 7.00 (m, 1H). ^{13}C NMR (100 MHz, $CDCl_3$)δ 149.72, 138.73, 137.93, 137.82, 136.54, 136.26, 135.22, 133.20, 130.31, 130.25, 129.23, 128.94, 128.80, 128.66, 128.31, 128.20, 127.39, 127.30, 126.48, 126.31, 125.99, 125.74, 125.30, 124.65, 124.08, 124.00, 123.93, 123.13, 122.12, 121.79, 119.89. MALDI-TOF (m/z): Calcd for $C_{47}H_{30}N_2$, 672.77; Found: 622.262 [M+].

PPIAnCz

The synthesis of **PPIAnCz** was similar to that of CrAn-Br. The synthetic route is shown in Scheme 1. PE/DCM (1:2, V/V) was used as the eluent and the resulting

product was recrystallized from DCM to give a pale yellow solid **PPIAnCz** in 40% yield.^{1}H NMR (600 MHz, $CDCl_3$) δ 8.91 – 8.87 (dd, J = 7.8, 1.8 Hz), 8.77 – 8.73(d, J = 8.4 Hz, 1H), 8.70 – 8.65 (d, J = 8.4 Hz, 1H), 8.14 (ddd, J = 8.4, 1.2, 0.6 Hz, 2H), 7.82 – 7.74 (m, 6H)， 7.72 (ddd, J = 13.8, 7.2, 1.2 Hz, 1H), 7.67 – 7.58 (m, 12H), 7.50 – 7.43 (m, 3H), 7.40 – 7.35 (m, 5H), 7.34 – 7.28 (m, 4H), 7.26 – 7.20 (m, 2H). ^{13}C NMR (100 MHz, $CDCl_3$)δ 149.05, 140.77, 140.44, 135.35, 135.12, 133.25, 133.01, 132.28, 130.37, 129.83, 129.27, 128.38, 127.93, 127.66, 126.32, 126.03, 125.79. MALDI-TOF (m/z): Calcd for $C_{59}H_{37}N_3$, 787.97; Found: 787.358 [M+].

3.Supplementary Figures

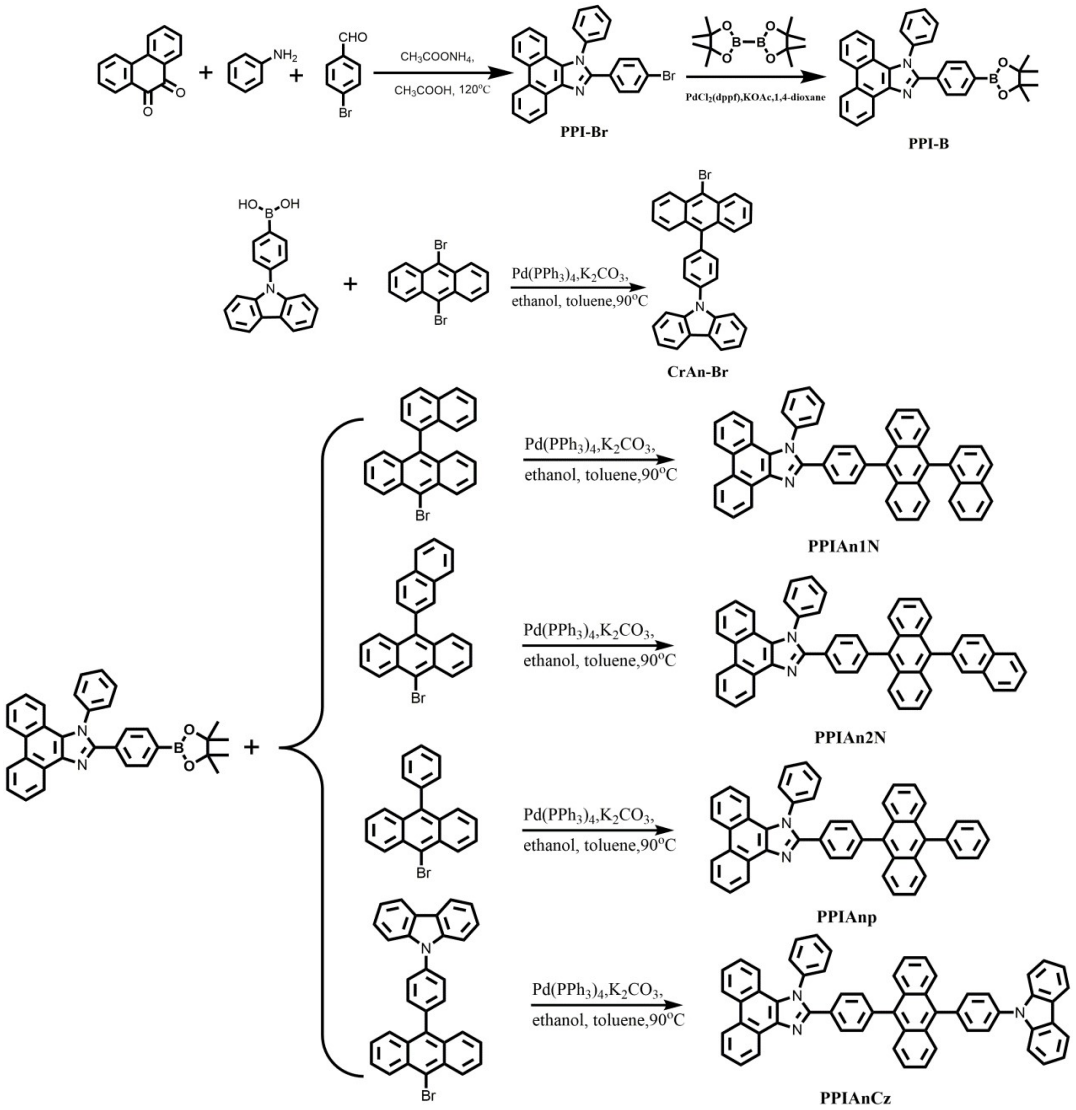

Fig.S1 Synthesis routes of **PPIAn1N**, **PPIAn2N**, **PPIAnp** and **PPIAnCz**

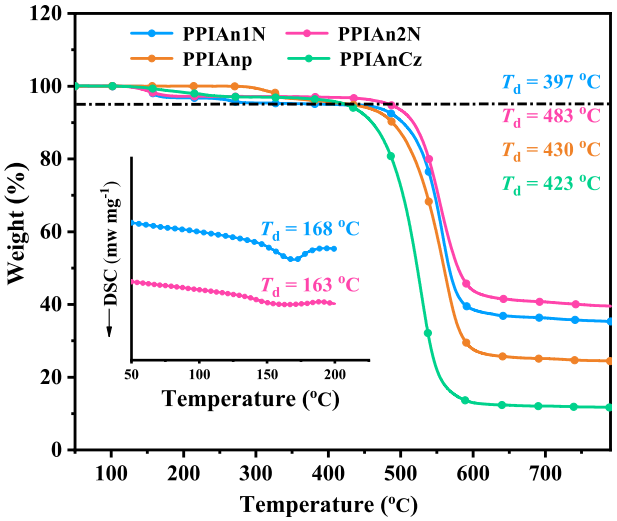

Fig.S2 TGA and DSC curves of **PPIAn1N**, **PPIAn2N**, **PPIAnp** and **PPIAnCz**

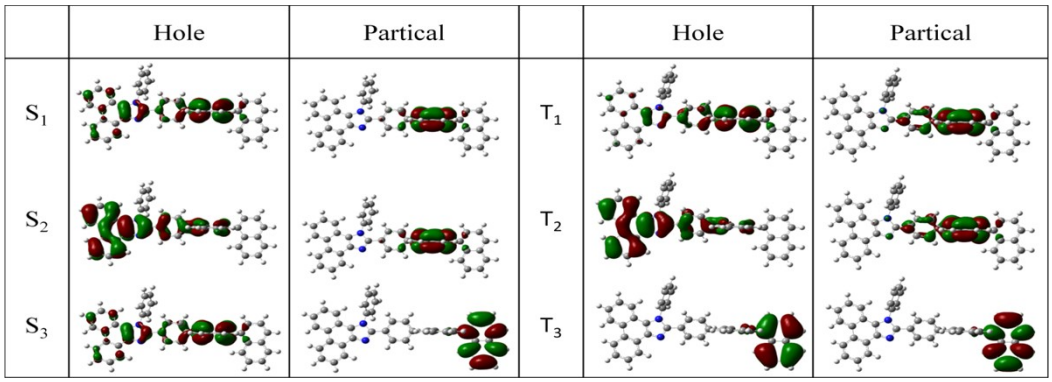

Fig.S3 NTOs of singlet and triplet excited states for **PPIAn1N**

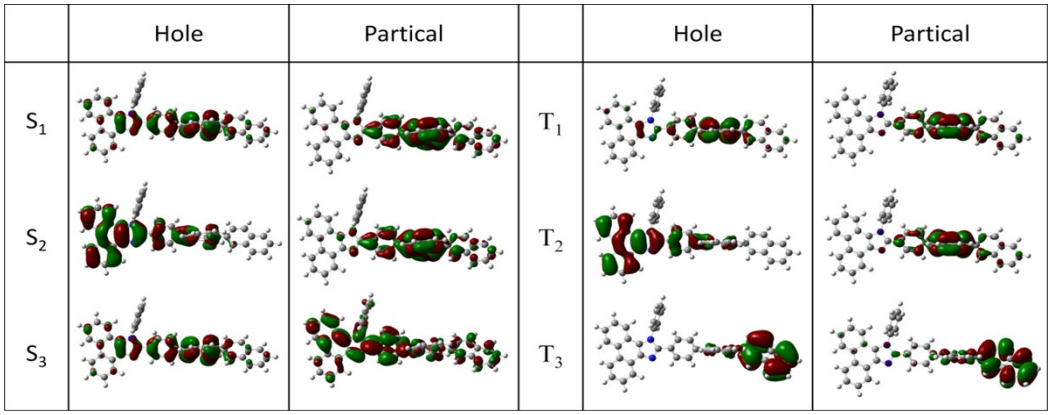

Fig.S4 NTOs of singlet and triplet excited states for **PPIAn2N**

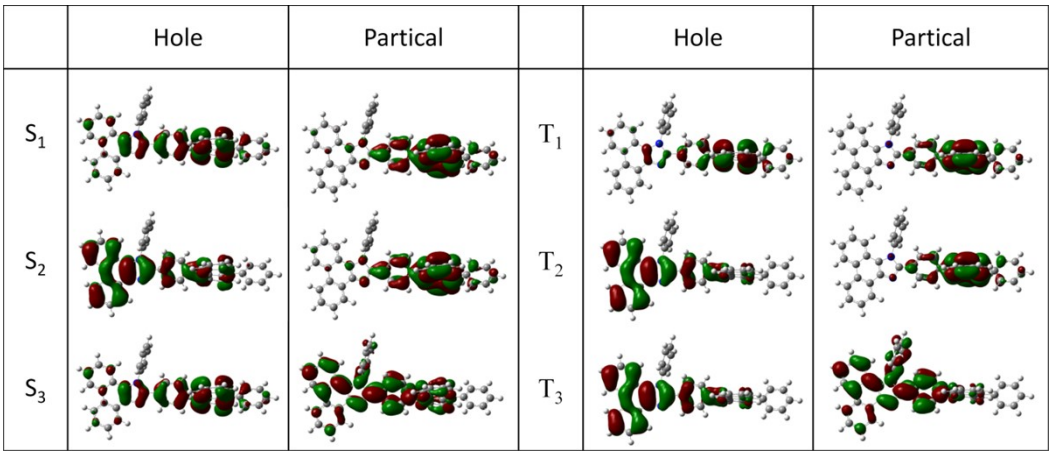

Fig.S5 NTOs of singlet and triplet excited states for **PPIAnp**

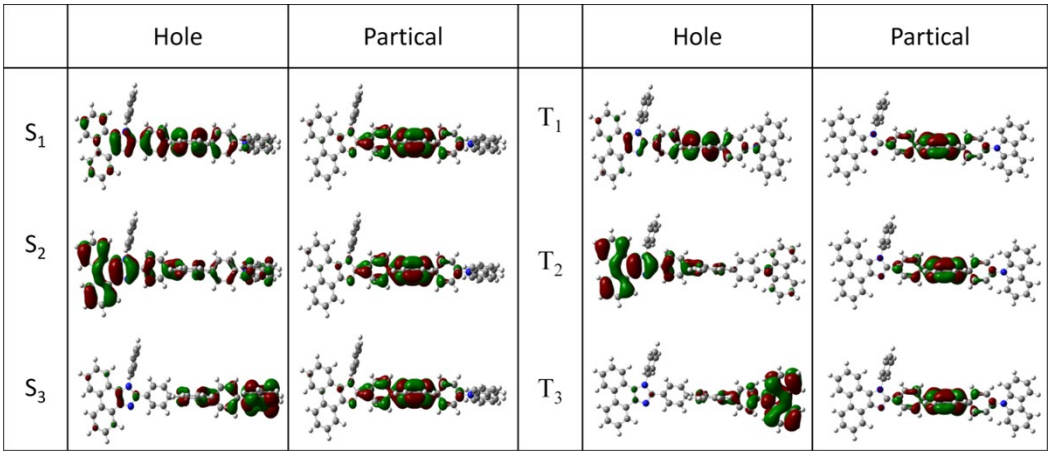

Fig.S6 NTOs of singlet and triplet excited states for **PPIAnCz**

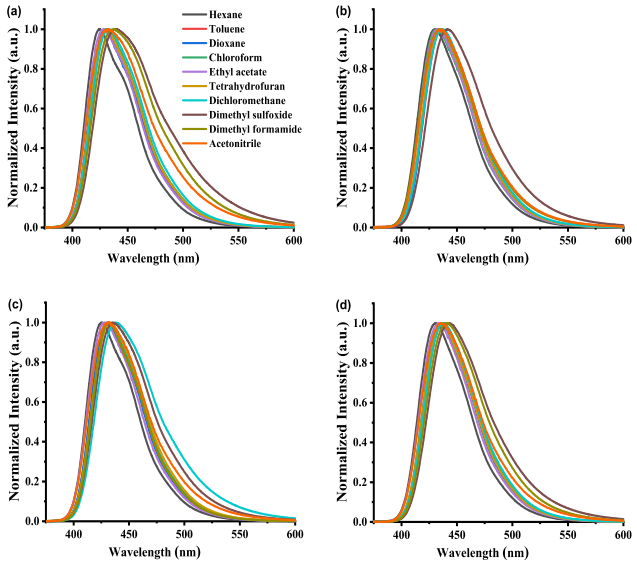

Fig.S7 PL spectra of **PPIAn1N** (a), **PPIAn2N** (b), **PPIAnph** (c) and **PPIAnCz** (d) in different solvents

Table.S1 Absorption and emission peaks of **PPIAn1N**, **PPIAn2N**, **PPIAnp** and **PPIAnCz** in different solvents (10^{-5} M)

Solution	$f(\varepsilon, n)$	**PPIAn1N**		**PPIAn2N**		**PPIAnP**		**PPIAnCz**	
		ν_a[a] (nm)	ν_f[b] (nm)	ν_a[a] (nm)	ν_f[b] (nm)	ν_a[a] (nm)	ν_f[b] (nm)	ν_a[a] (nm)	ν_f[b] (nm)
Hexane	0.0012	395	424	395	430	394	426	394	431
Toluene	0.012	398	431	398	437	397	431	397	437
Dioxane	0.021	397	430	397	434	397	430	397	434
Chloroform	0.149	397	432	397	432	397	432	398	437
Ethyl acetate	0.2	396	428	396	432	396	428	395	432
Tetrahydrofuran	0.21	397	431	397	435	396	434	397	436
Dichloromethane	0.217	397	433	397	437	397	438	398	438
Dimethyl sulfoxide	0.2632	399	440	399	442	398	436	399	442
Dimethylformamide	0.276	397	438	396	435	397	432	397	441
Acetonitrile	0.305	396	432	396	436	396	436	397	438

[a] absorption peak level, [b] emission peak level.

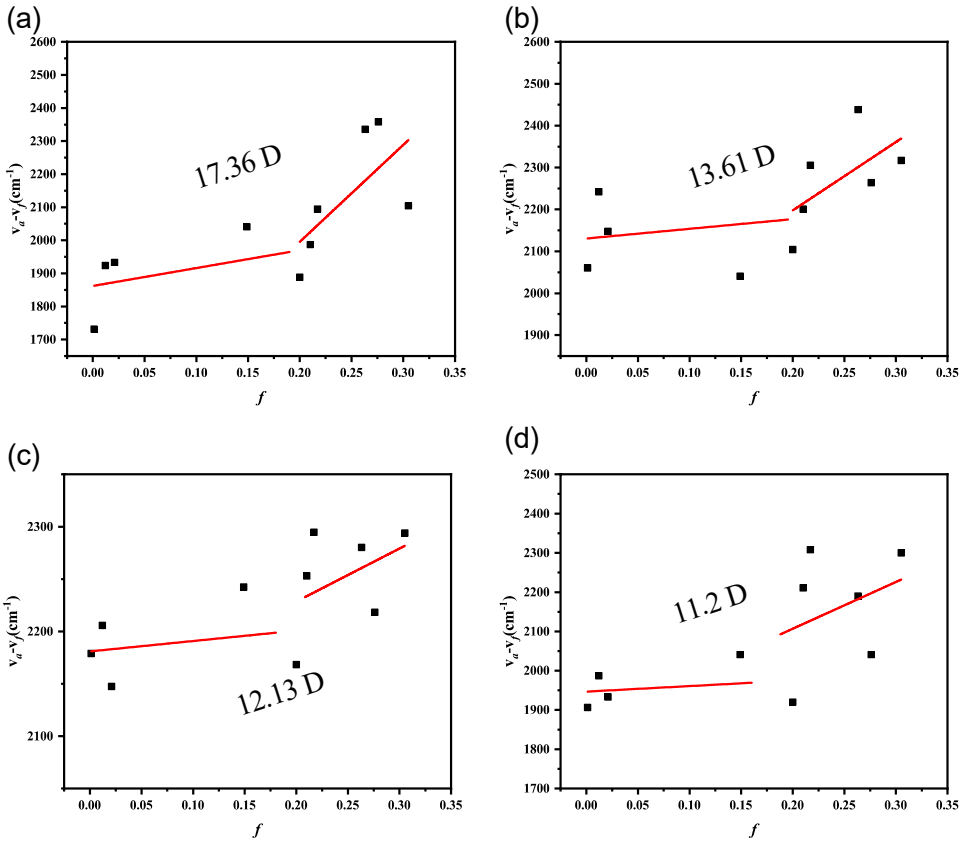

Fig.S8 Linear correlation of orientation polarization of solvent media with the Stokes shift ($v_a - v_f$) for **PPIAn1N** (a), **PPIAn2N** (b), **PPIAnp** (c) and **PPIAnCz** (d)

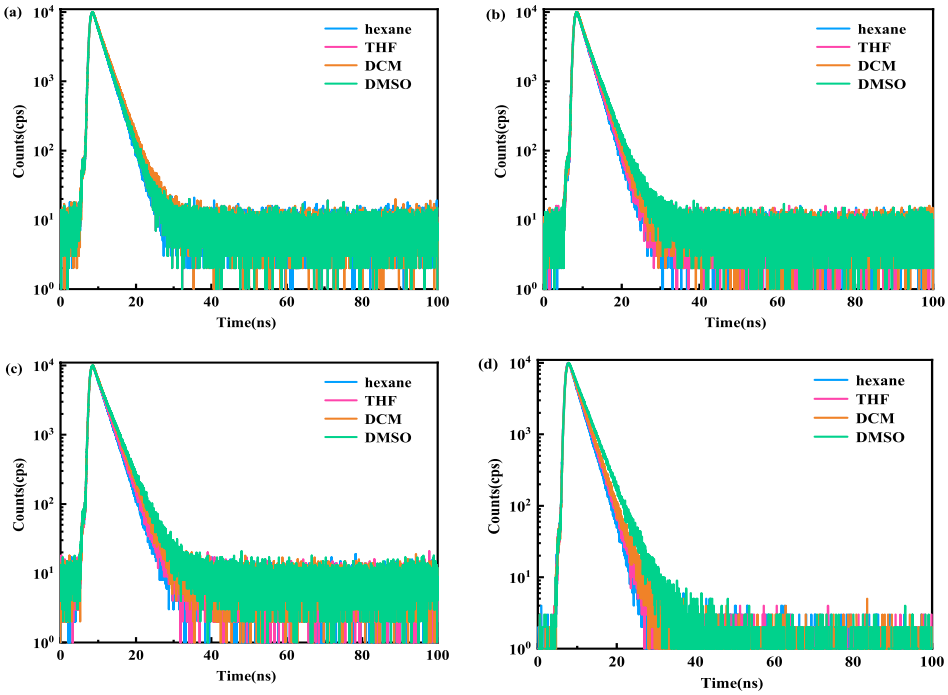

Fig.S9 decay curves of **PPIAn1N** (a), **PPIAn2N** (b), **PPIAnp**(c) and **PPIAnCz**(d) in different solvents

Table.S2 Lifetime measurement of **PPIAn1N**, **PPIAn2N**, **PPIAnp** and **PPIAnCz** in different solvents (ns)

Compound	hexane	THF	DCM	DMSO
PPIAn1N	2.47	2.54	2.75	3.10
PPIAn2N	2.33	2.42	2.56	2.77
PPIAnp	2.61	2.73	2.92	3.13
PPIAnCz	2.38	2.50	2.61	2.99

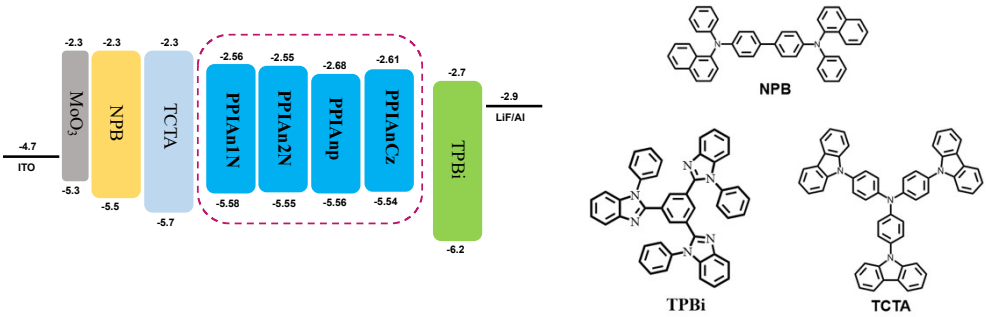

Fig.S10 The energy levels and molecular structure OLED devices

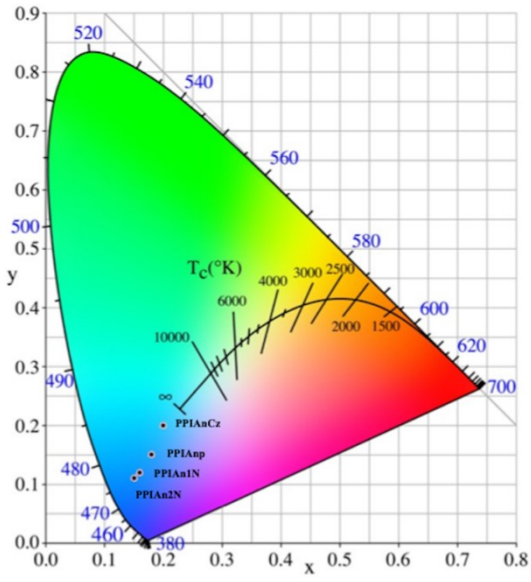

Fig.S11 CIE coordinates of OLEDs based **PPIAn1N**, **PPIAn2N**, **PPIAnp** and **PPIAnCz**

Table.S3 Hole and electron mobility of **PPIAn1N**, **PPIAn2N**, **PPIAnp** and **PPIAnCz**

Device	**PPIAn1N**	**PPIAn2N**	**PPIAnp**	**PPIAnCz**
μ_h/ （$cm^2\ V^{-1}\ s^{-1}$）	4.70×10^{-6}	6.46×10^{-6}	2.79×10^{-6}	4.00×10^{-6}
μ_e/ （$cm^2\ V^{-1}\ s^{-1}$）	2.18×10^{-10}	1.70×10^{-7}	1.4×10^{-7}	2.13×10^{-9}

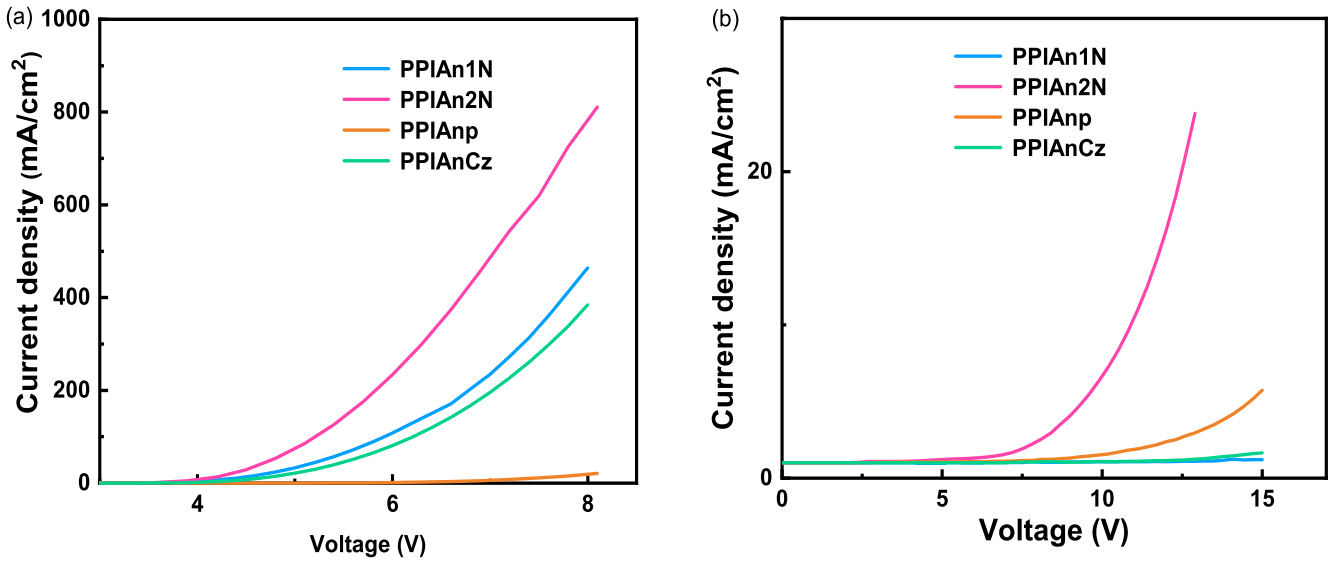

Fig.S12 Hole(a) and electron(b) single-carrier device current density-voltages curves for **PPIAn1N**, **PPIAn2N**, **PPIAnp** and **PPIAnCz**

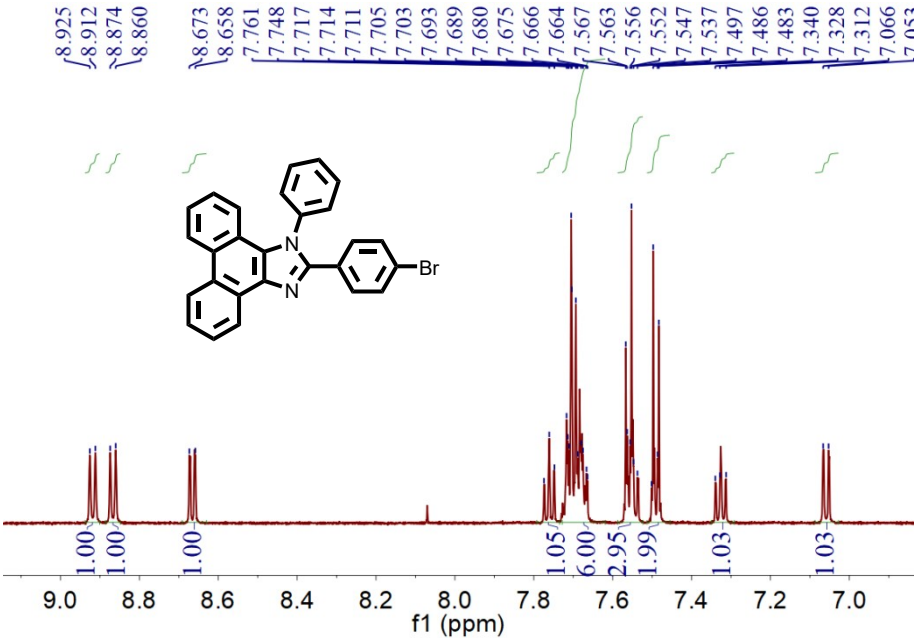

Fig.S13 ^{1}H NMR data of **PPI-Br** in DMSO

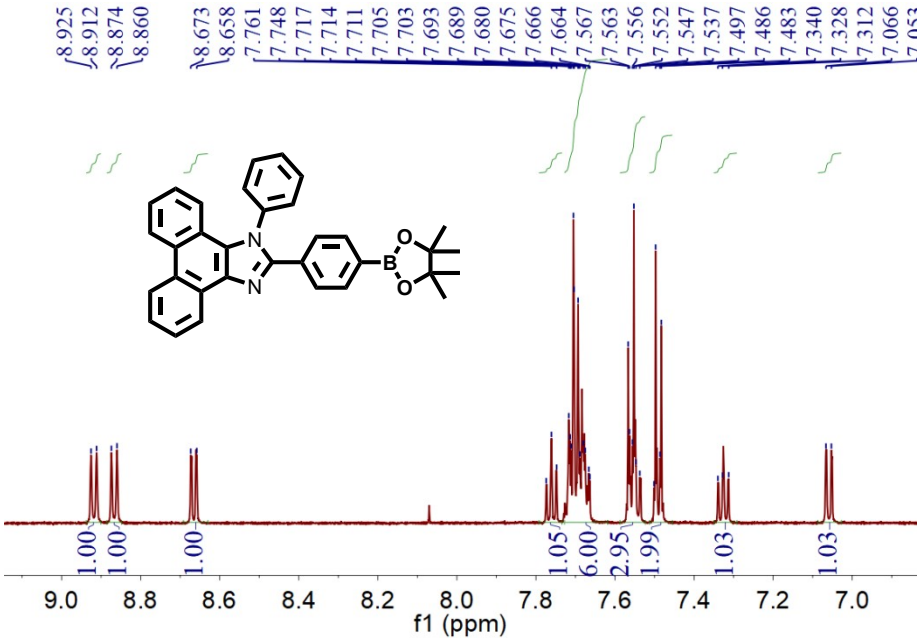

Fig.S14 ^{1}H NMR data of **PPI-B** in DMSO

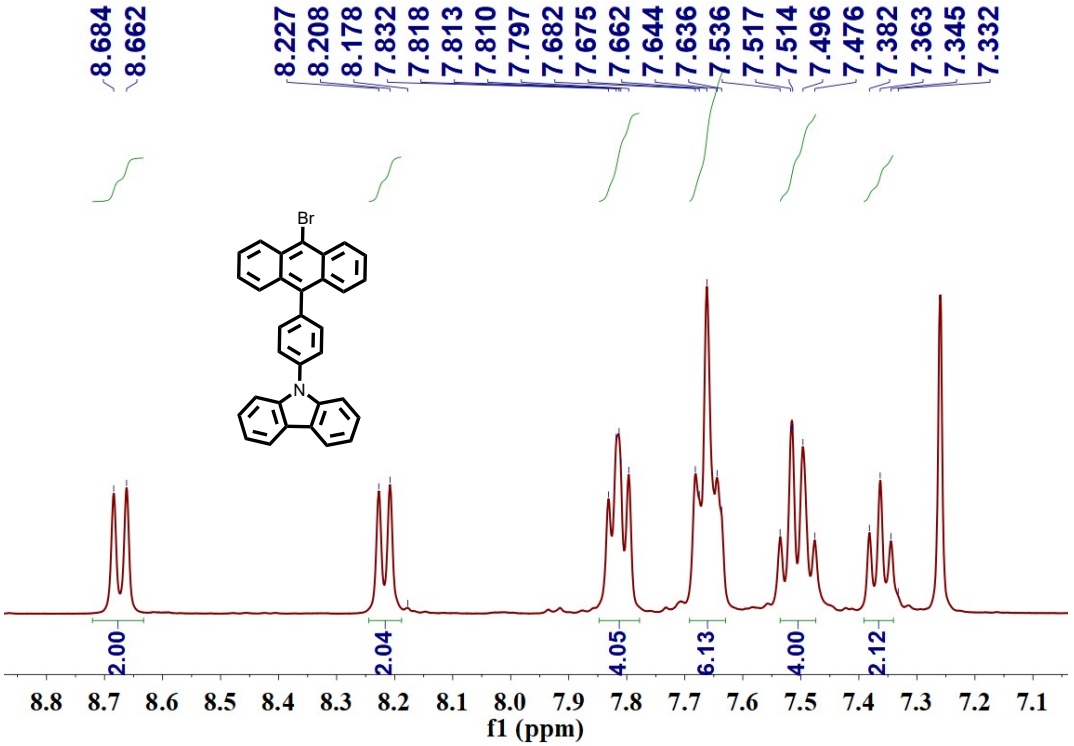

Fig.S15 ^{1}H NMR data of **CzAn-Br** in $CDCl_3$

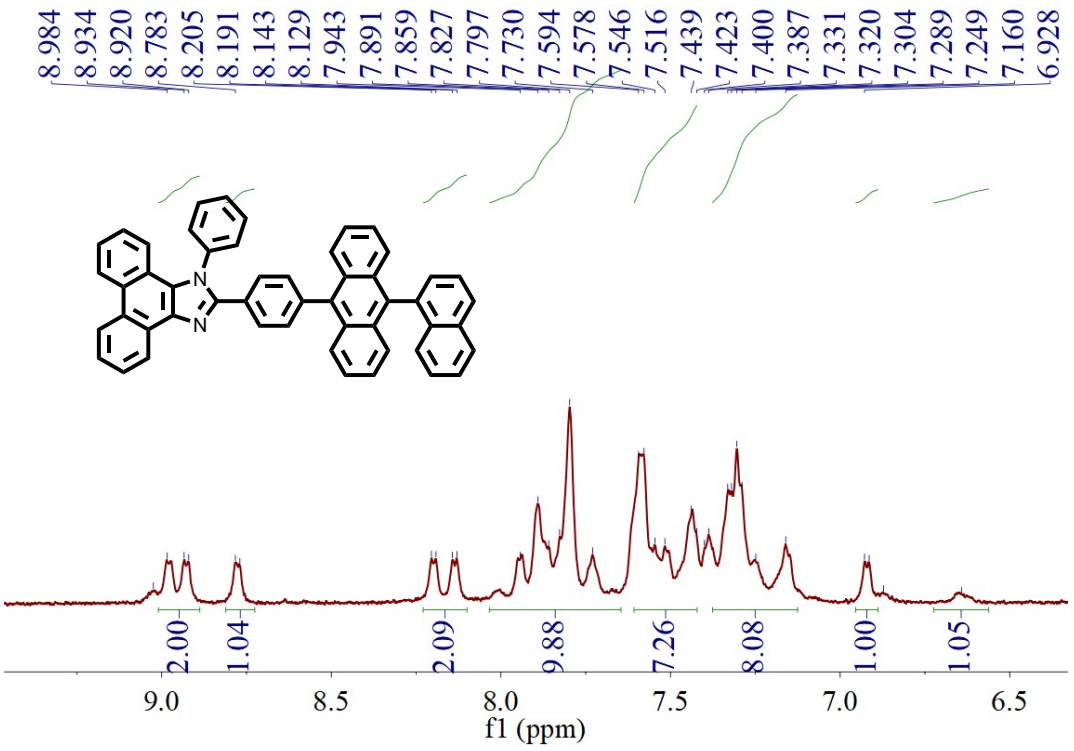

Fig.S16 ^{1}H NMR data of **PPIAn1N** in DMSO

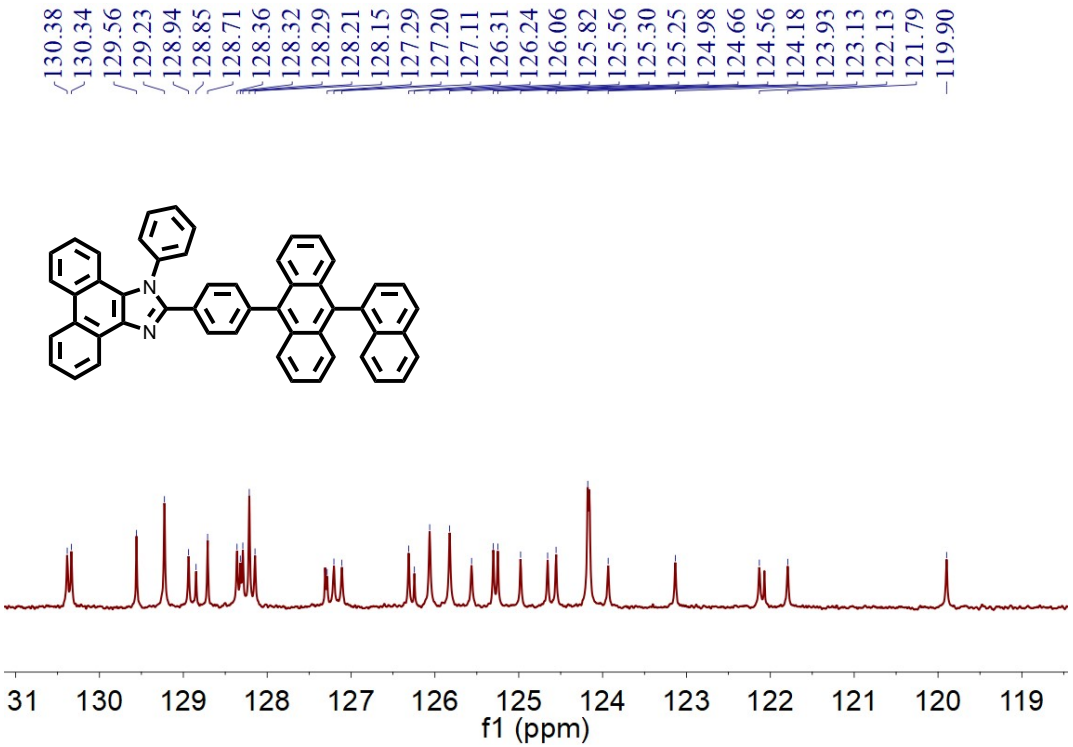

Fig.S17 ^{13}C NMR data of **PPIAn1N** in $CDCl_3$

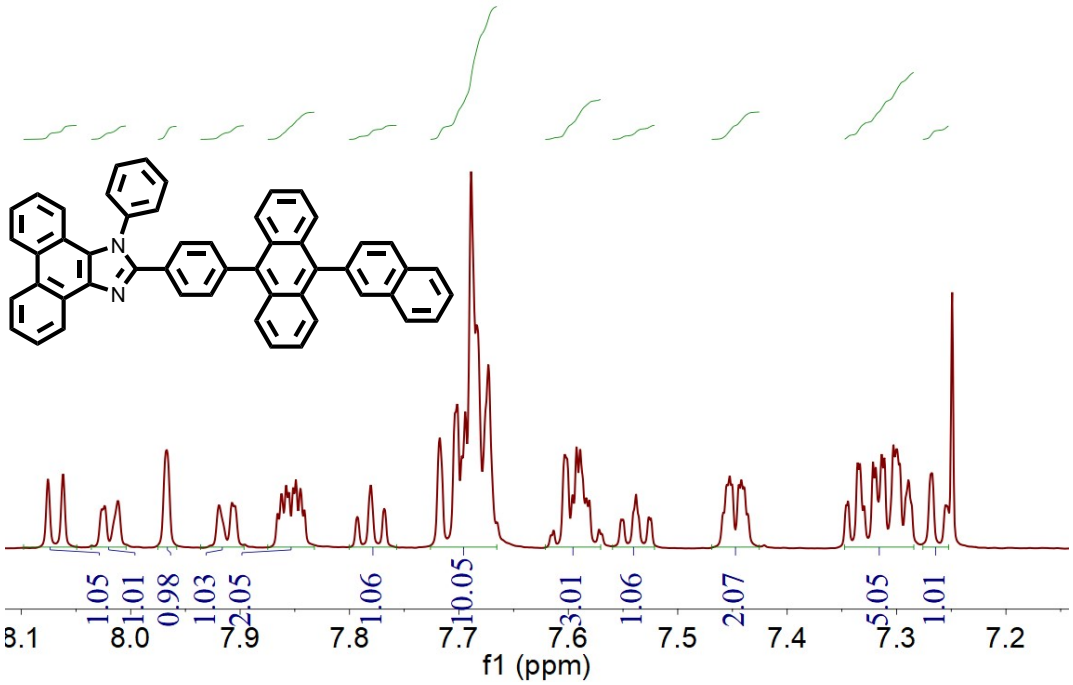

Fig.S18 ^{1}H NMR data of **PPIAn2N** in $CDCl_3$

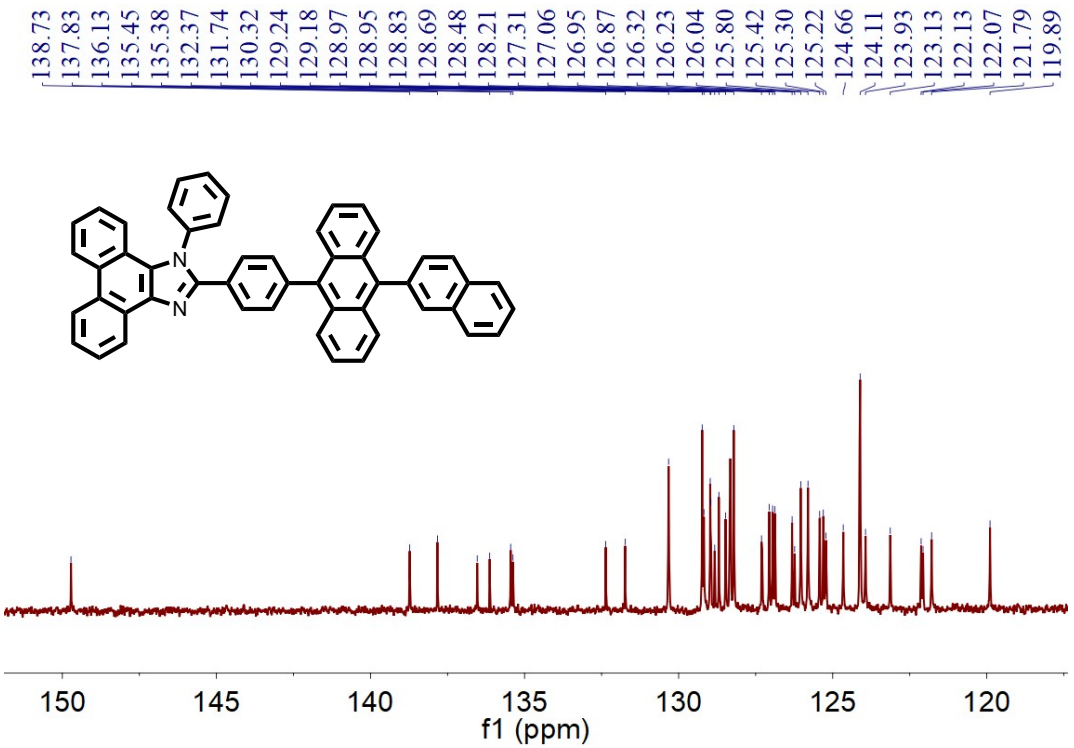

Fig.19 ^{13}C NMR data of **PPIAn2N** in $CDCl_3$

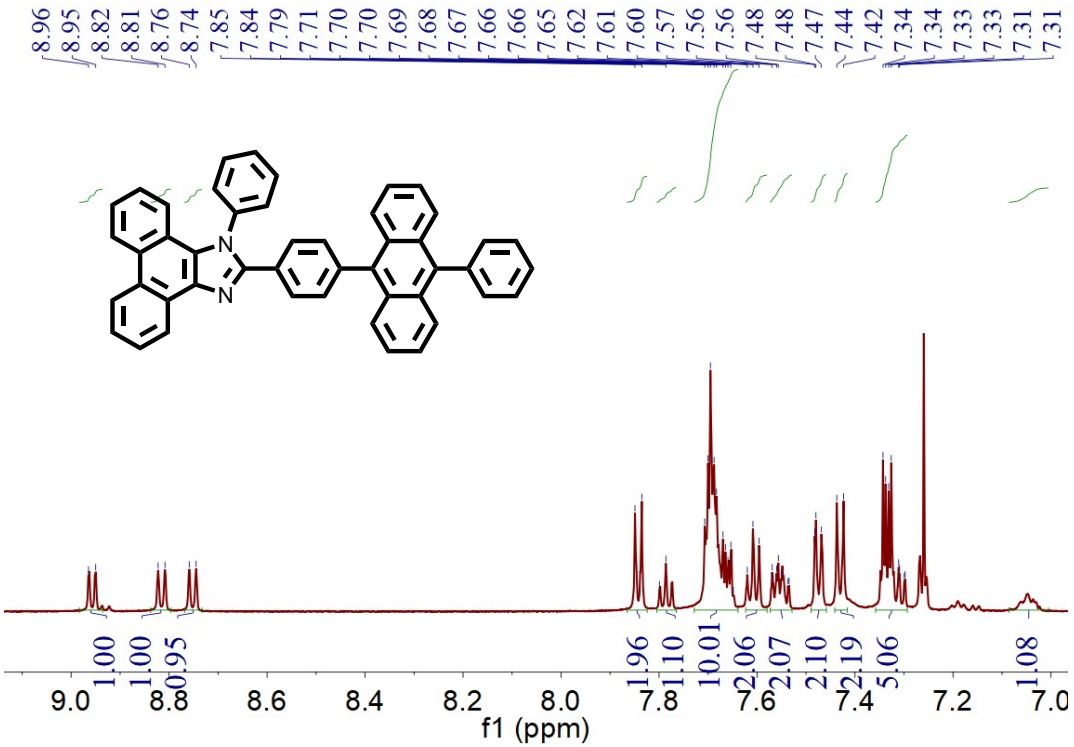

Fig.S20 ^{1}H NMR data of **PPIAnp** in $CDCl_3$

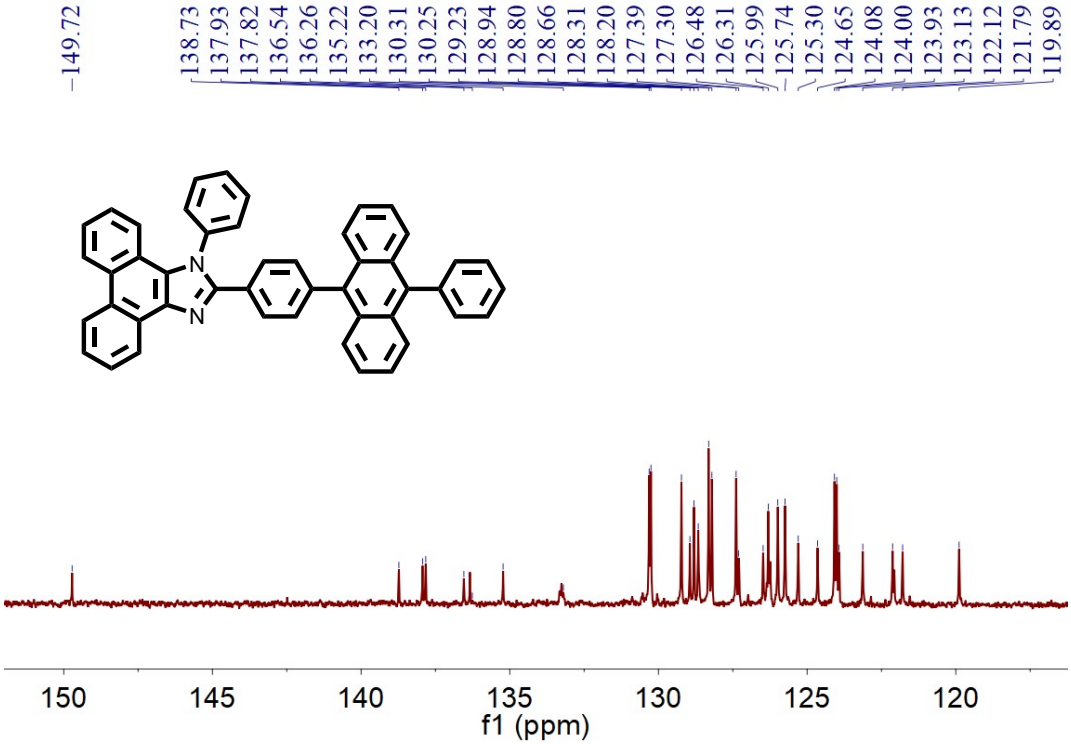

Fig.S21 ^{13}C NMR data of **PPIAnp** in $CDCl_3$

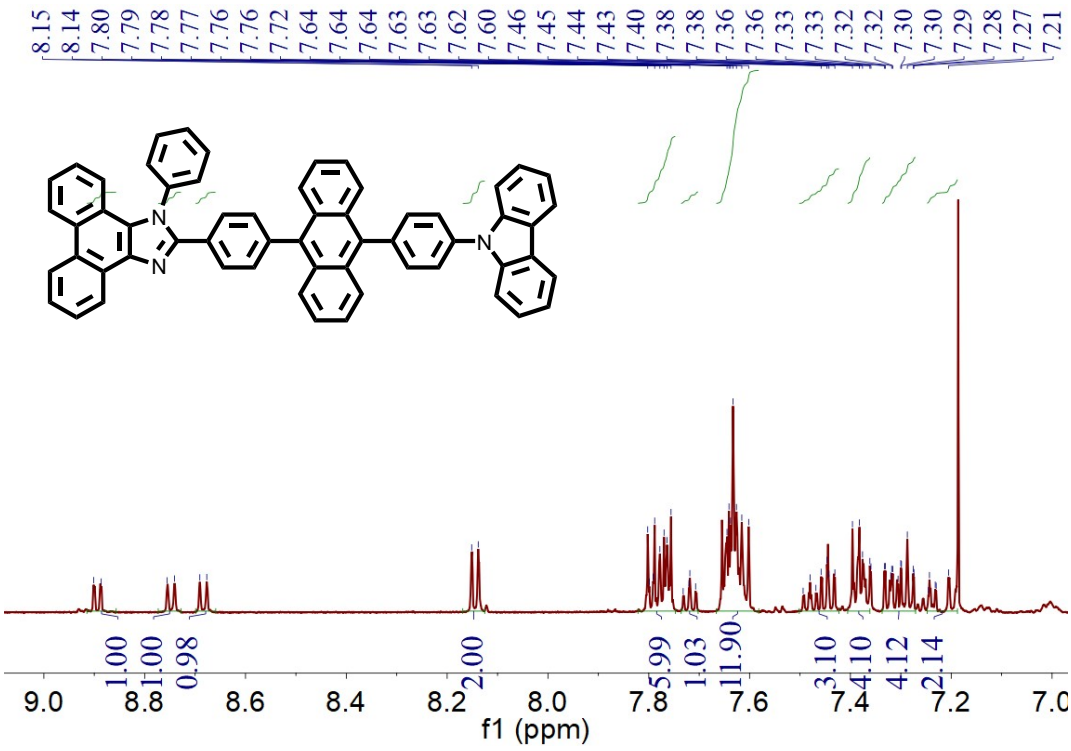

Fig.S22 ^{1}H NMR data of **PPIAnCz** in $CDCl_3$

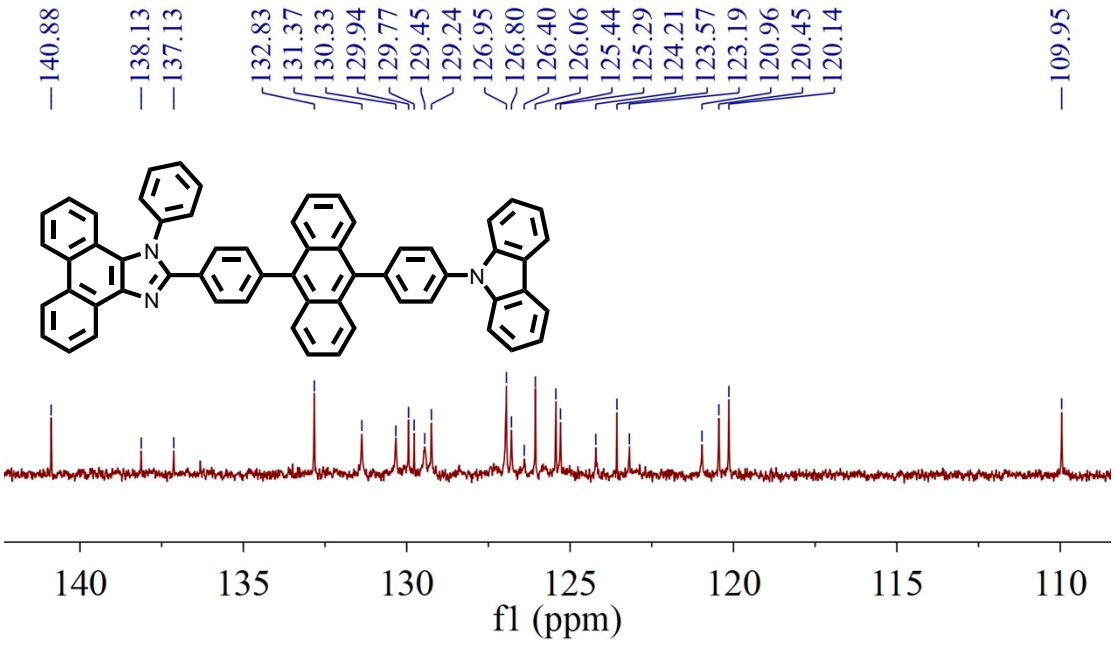

Fig.S23 ^{13}C NMR data of **PPIAnCz** in $CDCl_3$

Table.S4 Crystal Data and Structure Refinement for **PPIAn1N**,**PPIAn2N**,**PPIAnp** and **PPIAnCz**

Identification code	**PPIAn1N**	**PPIAn2N**	**PPIAnp**	**PPIAnCz**
Empirical formula	$C_{51}H_{32}N_2$	$C_{51}H_{32}N_2$	$C_{47}H_{30}N_2$	$C_{59}H_{37}N_3$
Formula weight	672.78	672.78	622.73	787.91
Temperature/K	150.00(10)	278(6)	149.98(10)	150.05(16)
Crystal system	monoclinic	monoclinic	triclinic	orthorhombic
Space group	I2/a	$P2_1/c$	P-1	Pbca
a / Å	26.0359(9)	15.0599(11)	9.3045(2)	7.72400(10)
b/ Å	9.0846(4)	9.2891(5)	9.6364(2)	31.3240(6)
c/ Å	32.8163(13)	26.6861(18)	18.4321(4)	34.0208(7)
α/°	90	90	88.296(2)	90
β/°	100.886(4)	103.037(7)	84.490(2)	90
γ/°	90	90	74.167(2)	90
Volume/ $Å^3$	7622.2(5)	3637.0(4)	1582.60(7)	8231.2(3)
Z	8	4	2	8
ρ_{calc} g/cm^3	1.173	1.229	1.307	1.272
μ/mm^{-1}	0.520	0.545	0.076	0.568
F(0 0 0)	2816.0	1408.0	652.0	3296.0
Crystal size / mm^3	0.04 × 0.02 × 0.02	0.06 × 0.04 × 0.03	0.17 × 0.15 × 0.14	0.07 × 0.03 × 0.02
2θ range for data collection/°	9.61 to 150.502	6.024 to 163.406	4.394 to 61.55	5.196 to 155.56
Radiation	Cu Kα (λ = 1.54184)	Cu Kα (λ = 1.54184)	Mo Kα (λ = 0.71073)	Cu Kα (λ = 1.54184)
Reflections collected	27342	23584	24715	28783
Goodness-of-fit on F^2	1.020	0.980	1.092	1.097
Final R	R_1 = 0.0527, wR_2 = 0.1329	R_1 = 0.0815, wR_2 = 0.2086	R_1 = 0.0426, wR_2 = 0.1170	R_1 = 0.0529, wR_2 = 0.1155

indexes[I≥2σ(I)]				
Final R indexes [all data]	R_1 = 0.0840, wR_2 = 0.1509	R_1 = 0.1693, wR_2 = 0.2673	R_1 = 0.0508, wR_2 = 0.1220	R_1 = 0.0692, wR_2 = 0.1235
Largest diff. peak/hole / e Å-3	0.23/-0.23	0.19/-0.26	0.35/-0.25	0.16/-0.20